Nanoscale

Accepted Manuscript

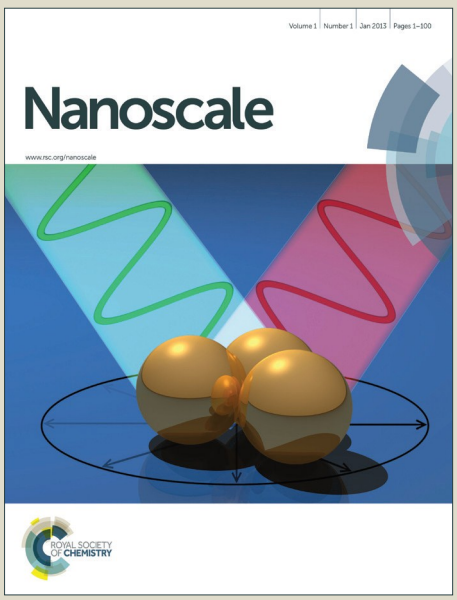

ROYAL SOCIETY OF CHEMISTRY

www.rsc.org/nanoscale

Nanoscale

RSCPublishing

ARTICLE

RNAi-based glyconanoparticles trigger apoptotic pathways for *in vitro* and *in vivo* enhanced cancer-cell killing

Cite this: DOI: 10.1039/x0xx00000x

João Conde[a,†], Furong Tian[b,†], Yulan Hernandez[c], Chenchen Bao[d], Pedro V. Baptista[e], Daxiang Cui[d], Tobias Stoeger[b*] and Jesus M de la Fuente[c,d,f*]

Received 00th January 2012,
Accepted 00th January 2012

DOI: 10.1039/x0xx00000x

www.rsc.org/

Gold glyconanoparticles (GlycoNPs) are full of promises in areas like biomedicine, biotechnology and material science due to their amazing physical, chemical and biological properties. Here, siRNA GlycoNPs (AuNP@PEG@Glucose@siRNA) in comparison to PEGylated GlycoNPs (AuNP@PEG@Glucose) were applied *in vitro* to a luciferase-CMT/167 adenocarcinoma cancer cell line and *in vivo* via intratracheal instillation directly into the lung of B6 albino mice grafted with luciferase-CMT/167 adenocarcinoma cells. siRNA GlycoNPs but not PEGylated GlycoNPs induced the expression of pro-apoptotic proteins such as Fas/CD95 and caspases 3 and 9 in CMT/167 adenocarcinoma cells in a dose dependent manner, independent from the inflammatory response, evaluated by bronchoalveolar lavage cell counting. Moreover, *in vivo* pulmonary delivered siRNA GlycoNPs were capable of targeting *c-Myc* gene expression (a crucial regulator of cell proliferation and apoptosis) via *in vivo* RNAi in tumour tissue, leading to a ~80% reduction in tumour size without inflammation associated.

Introduction

Carbohydrates are, together with nucleic acids and proteins, important molecules for life. Although individual carbohydrate interactions are relatively weak, nature utilized multivalent interactions between these cell surface ligands and their respective biological receptors to modulate biological events such as the ones related to cell adhesion, normal tissue growth and repair, viral/bacterial infection, signal transduction, trapping of leukocytes, and gene transfer. So the decoding of carbohydrate interactions opens up the possibility to employ physiologically inert gold nanoclusters in diagnostics and/or therapy.[1] Among them, gold glyconanoparticles (GlycoNPs) have drawn more attention owing to their well-defined features as water-soluble carbohydrate-functionalized nanoclusters with a promising potential for chemical glycobiology, biomedicine, diagnostics and clinical applications. In the last 10 years, de la Fuente and co-workers have extensively reported a pioneered integrated glyconanotechnology strategy based on the use of nanoparticles to study and evaluate carbohydrate–carbohydrate, carbohydrate–protein interactions [2-6] and used as potential tools in anti-adhesive therapy [7], for cell-cell adhesion studies [8] and for the prevention of pathogen invasion.[9]

Small carbohydrates such as glucose can be attached to gold nanoparticles (AuNPs) and may be useful mainly in sensitive colorimetric assays.[10] However, to the best of our knowledge the use of siRNA GlycoNPs for the regulation of important genes of the apoptotic pathways has never been described so far.

Herein, a novel structure of multifunctional RNAi-based GlycoNPs functionalized with glucose, poly(ethylene glycol) (PEG), a biotin linked fluorophore and cMyc targeting siRNA were designed to trigger apoptosis and gene silencing pathways (see **Figure 1**). Via a chemical approach, the functional properties and moieties of this kind of multifunctional nanostructure can be easily tuned and quantified as recently reported by our group.[11,12] In fact, we have provided evidence of *in vitro* and *in vivo* efficient RNAi via the synthesis of a library of novel multifunctional AuNPs, tested in three biological systems of increasing complexity: *in vitro* cultured human cells (HeLa cells), *in vivo* freshwater polyp (*Hydra vulgaris*), and *in vivo* mice models (B6 albino mice).[11,13]

In view of the great number of studies concerning glucotoxicity attributed to the inability of cells to reduce glucose uptake when exposed to chronic hyperglycemia, we designed novel siRNA GlycoNPs that predispose gene expression to apoptosis via enhancement of cell death receptors. In fact, it is known that high levels of glucose induces apoptosis via upregulation of cell death receptors – Fas – providing a link between type 1 and type 2 diabetes.[14,15] Hyperglycemia is the central initiating factor for all types of diabetic microvascular disease. Studies in endothelial cell cultures clearly show glucose toxicity by delaying replication, disturbing cell cycle, increasing DNA damage and accelerating cell death.[16,17]

Nanoscale RSCPublishing

ARTICLE

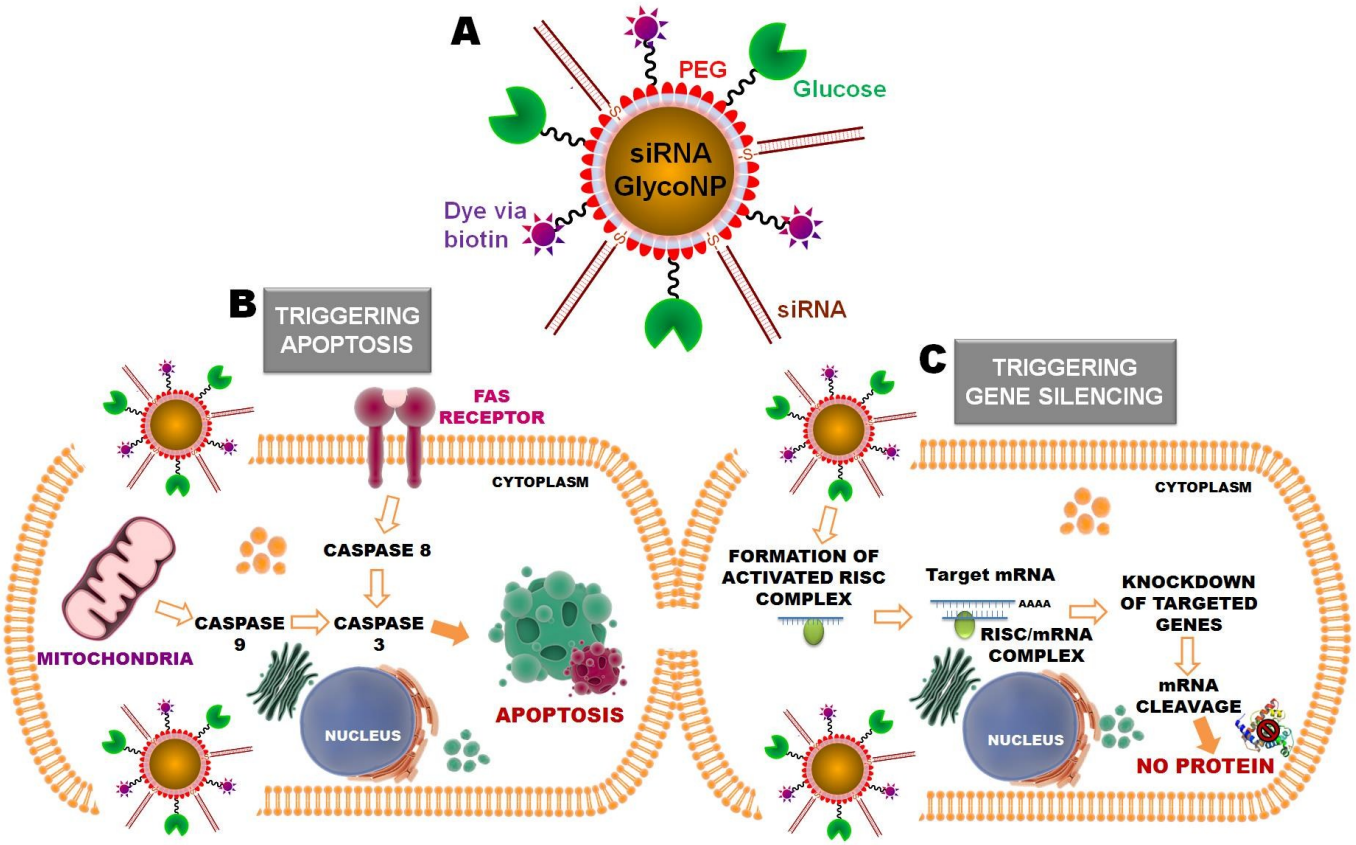

Figure 1. (**A**) Multifunctional siRNA Glyconanoparticles (siRNA GlycoNPs) trigger apoptotic pathways (**B**) with expression of cell death receptors (Fas) and caspases. The death domain-containing receptor Fas can sense an external signal and activate the apoptosis pathway through the Fas-related death domain. This pathway is mediated by the activation of caspase-8, followed by direct cleavage of downstream effector caspases. The apoptosis pathway can also be initiated cytoplasmatic, through activation of intracellular changes resulting in the release of proapoptotic factors from the mitochondria. The release of these factors leads to the activation of caspase-9, and ultimately results in the activation of effector caspases (e.g. caspase 3) and consequently to cell death by apoptosis. (**C**) The siRNA glycoNPs have also the capacity to trigger gene silencing via activation of the RNA interference pathway, by double-stranded RNA (i.e. siRNA), promoting nucleolytic degradation of the target mRNA and/or translational suppression.

Maedler et al. also reported that increased glucose concentration by itself induces apoptosis in human pancreatic β-cells via the upregulation of Fas receptors, which can interact with the constitutively expressed FasL (Fas ligand) on neighbouring β-cells. Fas-FasL interaction leads to cleavage of procaspase-8 to caspase-8, which promotes caspase-3 activation.[14] The stimulation of death receptors such as Fas (APO-1/CD95) and creation of DISC (death-inducing signalling complex) are commonly referred as the starting point in the extrinsic apoptosis execution phase; whereas caspase-9 activation is a downstream marker for mitochondrial membrane permeabilisation, in the intrinsic apoptotic pathway.[18] Both pathways converge on the same terminal outcome, which is initiated by the cleavage of caspase-3 and results in DNA fragmentation, degradation of cytoskeletal and nuclear proteins, formation of apoptotic bodies, expression of ligands for phagocytic cell receptors and finally clearance by phagocytic cells.

Herein, the *in vitro* and *in vivo* activation of apoptotic and gene silencing pathways via RNAi GlycoNPs will be dissected and the clinical outcome in terms of lung cancer progression evaluated.

Results and discussion

Glyconanoparticles synthesis and characterization

Multifunctional gold glyconanoparticles were prepared by reduction of sodium tetracholoroaurate(III) hydrate with sodium citrate as described by *Turkevich* and *Frens* [19,20], and stabilized with polyethyleneglycol (PEG) and subsequent conjugation with glucose, biotin and siRNA. Briefly, the obtained AuNPs, with an average diameter of 14 nm, were subsequently functionalized with two types of thiolated poly(ethylene glycol) (PEG) – a commercial carboxylated PEG (HS-EG(8)-$(CH_2)_2$-COOH) and another one synthesized in our lab with an azide group at the end (HS-$(CH_2)_3$-CONH-EG(6)-$(CH_2)_2$-N_3) - by exchange of the citrate groups,. For the subsequent attachment of thiolated siRNA using the covalent approach previously described [11], the AuNPs were functionalized with a 40% degree of coverage of the surface using 50% of each PEG chain.

Once obtained stable and biocompatible PEGylated AuNPs we functionalized them with amine-modified biotin and glucose through an EDC coupling reaction forming amide bonds with the carboxylic groups exposed on the surface. The covalent conjugation of the biotin was evaluated by the crosslinking induced by the effective attachment of streptavidin to up to four biotin molecules and also determined by indirect quantification by the Bradford assay. Concerning the attachment of glucose, the change of the net charge and the aggregation of the AuNPs effectively functionalized in the presence of the lectin Concanavalin A [21] were used to confirm the conjugation, again via the occurrence of crosslinking induced due to the multi-interaction between glucose and Con A. Lastly, GlycoNPs were functionalized with thiolated anti *cMyc* siRNA through direct attach of the thiol group to the gold core of the AuNP by establishing strong pseudo-covalent bonds Au-S (for further details see Supplementary Information)

Triggering apoptotic pathways via glyconanoparticles

The functionalized nanoparticles were administered *in vitro* to a luciferase-CMT/167 adenocarcinoma cancer cell line and *in vivo* via instillation directly into the lung of cancer mice (B6 albino mice, induced with luciferase-CMT/167 adenocarcinoma cells). 48 hours upon treatment with increasing concentrations (10, 100 and 200 µg/mL) of PEGylated GlycoNPs (AuNP@PEG@Glucose) and siRNA GlycoNPs (AuNP@PEG@Glucose@siRNA) cells were assessed for the expression of proapoptotic genes such as Fas/CD95 and caspases-3 and -9, as well as the siRNA target *c-Myc* gene, that also triggers apoptosis in association with tumour suppressors such as ARF and p53.[22]

Representative confocal images of LA-4 adenocarcinoma-loaded cells show that siRNA GlycoNPs accomplish high cellular uptake (3-fold) and trigger apoptosis by enhancing the expression of Fas death receptor, as detected by a significant increase (2-fold) of Fas/CD95 fluorescence (**Figure 2A**).

Glucose-surface functionalization has also been developed for siRNA GlycoNPs as a metabolic transporter to enhance the uptake of the therapeutic nanoparticles by cancer cells. In fact, tumour cells display a high rate of glucose uptake and glycolysis, since cell proliferation requires increased uptake of nutrients (e.g. glucose and glutamine). Cancer cells exhibit a high rate of glycolysis even in the presence of oxygen (aerobic glycolysis). The major function of aerobic glycolysis is to maintain high levels of glycolytic intermediates to support anabolic reactions in cells. This explains increased glucose metabolism in proliferating cells.[18] In addition to cell proliferation, increased glucose uptake may also be associated with mitochondria damage in cancer cells, or an adaptation to hypoxia environments within tumours or to mitochondria shutdown by cancer genes (eg. *c-Myc*) involved in the cell's apoptosis program.[24] In fact, high glucose levels proved to be pro-apoptotic, increasing the sensitivity to apoptosis via Fas activation.[14]

Our results suggest that siRNA GlycoNPs activate apoptotic pathways by regulating cell death receptors and effective caspases, and the effect is dose dependent. Increasing concentrations (10, 100 and 200 µg/mL) of siRNA GlycoNPs show enhancement in Fas expression in a dose dependent manner, as it can be seen by increase of Fas/CD95 fluorescence (see **Figure 2B**) in a 1.5-fold from 10 to 100 µg/mL and in a 3-fold from 100 to 200 µg/mL of NPs.

In order to corroborate these data and evaluate siRNA GlycoNPs' involvement in the activation of crucial proapoptotic proteins, expression of Fas, caspase-3 and caspase-9 was assessed by Western blot in luciferase-CMT/167 adenocarcinoma cancer cell line. The expression of Fas, activated/cleaved caspase-3 and caspase-9 proteins was significantly higher (5 fold) for siRNA GlycoNPs at 10, 100 and 200 µg/mL compared to PEGylated GlycoNPs (**Figure 3A**).

The expression of Fas and caspases-3 from cell treated with 10 µg/mL of siRNA GlycoNPs indicates the strong activation of both intrinsic and extrinsic apoptotic pathways. Enhanced activation of caspase-9 by siRNA GlycoNPs can especially be observed at 200 µg/mL (see **Figure 2**), which in turn may induce the activation of procaspase-3, which leads to the apoptosome formation.[25] Once formed, the apoptosome can then recruit and activate the inactive pro-caspase-9, which can activate effector caspases and trigger a cascade of events leading to apoptosis. Finally, after the activation of caspase-9, the effector caspase-3 is activated and marks the endpoint of apoptosis.[25]

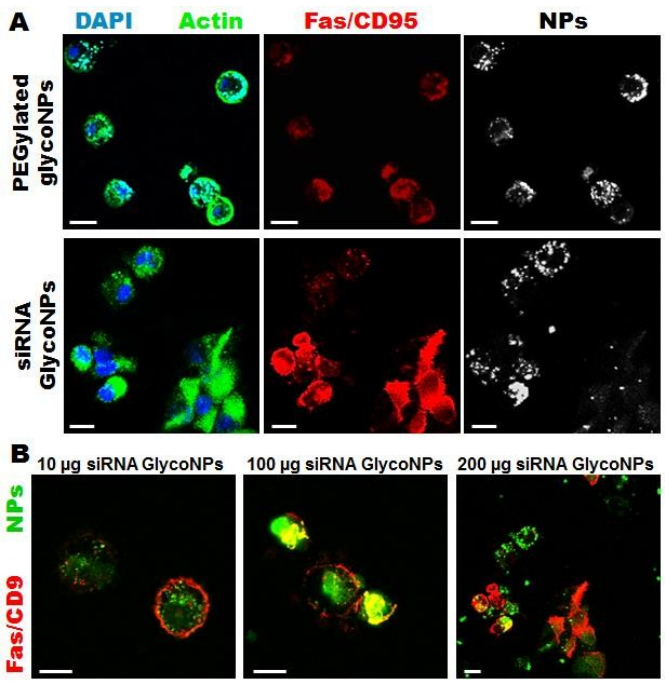

Figure 2. Gold siRNA glyconanoparticles trigger apoptotic pathways via expression of the Fas cell death receptor. (**A**) Immunostaining of Fas/CD95 in luciferase-CMT/167 adenocarcinoma cells treated with 200 µg/mL of PEGylated glycoNPs and siRNA GlycoNPs for 48 hours. Cells stained for DAPI (nuclei) in blue, actin (phalloidin) in green, Fas/CD95

stained in red and NPs (conjugated streptavidin with Cy7-Allophycocyanin bound with biotin) in white (Scale bars, 20 µm). (**B**) Immunostaining of Fas/CD95 in luciferase-CMT/167 adenocarcinoma cells treated with 10, 100 and 200 µg/mL of siRNA GlycoNPs. Cells stained for Fas/CD95 stained in red and NPs (conjugated streptavidin with Cy7-Allophycocyanin bound with biotin) in green (Scale bars, 20 µm). The results shown are representative for at least three independent experiments.

This finding further supports the notion that siRNA GlycoNPs promote apoptosis within the LA-4 adenocarcinoma cancer cell line when exposed for 48 hours at a concentration of 100 and 200 µg/ml (**Figure 3A,C**). PEGylated GlycoNPs showed no changes in expression of the assessed cell death receptor or caspases (**Figure 3A,C**).

RNAi-based GlycoNPs were also functionalized with a siRNA to mediate silencing of *c-Myc* gene expression. *c-Myc* is widely known as a crucial regulator of cell proliferation in normal and neoplastic cells, and recent reports strongly support a dual function model for *c-Myc* as a co-ordinate activator of cell proliferation and apoptosis.[28] Several studies provide evidences that *c-Myc* function is closely related to apoptosis and that the induction or inhibition of apoptosis by this protein may depend on the level of expression or cell lineages used.[28-30] To assess whether anti-cMyc siRNA GlycoNPs attenuate MYC protein synthesis, its expression was also evaluated by western blot in luciferase-CMT/167 adenocarcinoma cancer cell line (**Figure 3B,C**) after exposure to PEGylated GlycoNPs and siRNA GlycoNPs. Western blot results clearly show that *c-Myc* donwregulation (14-fold) is attained with only 10 µg/mL of siRNA GlycoNPs (**Figure 3B,C**). PEGylated GlycoNPs show no silencing effect for all NPs concentration (**Figure 3B,C**).

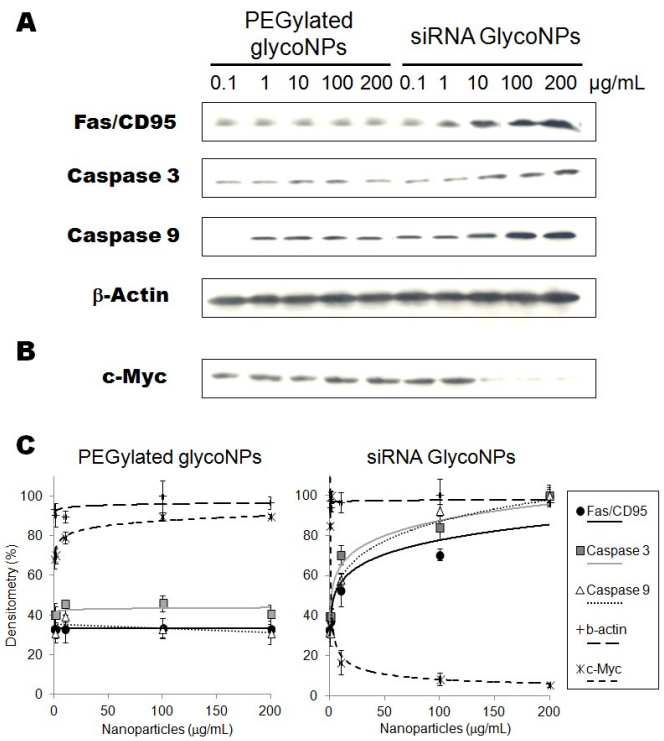

Figure 3. Activation of apoptotic pathway via siRNA GlycoNPs. Fas, Caspase 3, Caspase 9 (**A**) and *c-Myc* expression (**B**) in Western blot after LA-4 adenocarcinoma cancer cells treated with increasing concentrations (0.1, 1, 10, 100 and 200 µg/mL) of PEGylated GlycoNPs and siRNA GlycoNPs. (**C**) Comparative graph with the expression of Fas, and activated Caspases 3 and 9 and *c-Myc* after LA-4 adenocarcinoma cancer cells treated with PEGylated GlycoNPs and siRNA GlycoNPs. The results shown are representative for at least three independent experiments.

In vivo RNAi triggering via siRNA glyconanoparticles

For *in vivo* evaluation of GlycoNPs treatment on *c-Myc* expression in a mouse lung tumour model, 200 µg/mL of PEGylated GlycoNPs and siRNA GlycoNPs were administered to mice previously induced with luciferase-CMT/167 adenocarcinoma cells. Four weeks after orthotropic lung cancer induction mice were treated by instillation of 0.3 pmol AuNP (at weeks 12, 13, 14 and 15), respectively, in 50 µl pyrogene-free distilled water, followed by 100 µl of air. **Figure 4A** shows Hematoxylin and Eosin staining (H&E) and immunolocalisation of *c-Myc* expression in mice lung tissues for Sham, PEGylated GlycoNPs and siRNA GlycoNPs groups. PEGylated GlycoNPs treated group demonstrates a cancer lung tissue characterized by hypercellularity and thickened alveolar septa. Cancer cell have spread throughout the lung tissue, and large areas of deformed lung structures can be observed (**Figure 4A**). Severe interstitial inflammatory cell infiltration is noted in the PEGylated GlycoNPs treated group, with predominance of perivascular and peribronchiolar edemas (**Figure 4A** arrows). In the siRNA GlycoNPs-treated group in contrast a significant decrease in the incidence and severity of tumour foci in lung can be observed, revealing the potency of siRNA GlycoNPs in reducing the tumour mass in the lung cancer mouse model. Only few, scattered cancer cells can get localized with recovered alveolar lung tissue. Concerning confocal images of lung tissue, **Figure 4B** shows high expression of MYC protein in cytoplasm of tumour cells after exposure to PEGylated GlycoNPs. Whereas, **Figure 4C** illustrate tumour cells treated with siRNA GlycoNPs and shows downregulation of local MYC expression (6-fold), probably leading tumour cells to apoptosis, and consequently inhibiting cell proliferation. Moreover, cancer cells in lung tissue accumulate more siRNA GlycoNPs (2-fold) (**Figure 4C**) than PEGylated GlycoNPs (**Figure 4B**). Xing and co-workers also reported that glucose and antisense oligodeoxynucleotides-capped AuNPs showed significantly increased cellular uptake compared to neutral nanoparticles in breast cancer [30] and prostate cancer cells.[31]

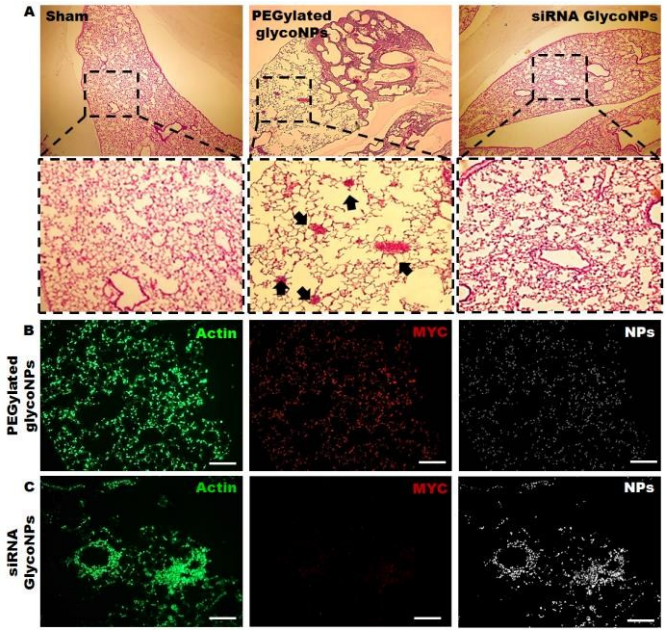

Figure 4. RNAi triggering in mice. (**A**) Hematoxylin and eosin (H&E) stains of Sham (healthy mice without lung cancer induction of luciferase-CMT/167 adenocarcinoma cells), PEGylated GlycoNPs and siRNA GlycoNPs treated groups in lung tissue with induction of LA-4 adenocarcinoma cells. Severe interstitial inflammatory cell infiltration is noted, with predominance of perivascular and peribronchiolar edemas (arrows) in PEGylated GlycoNPs only. Immunohistochemical images of lung tissue of PEGylated GlycoNPs (**B**) and siRNA GlycoNPs (**C**) treated groups. Cells in lung tissue stained for actin in green and MYC stained in red (Scale bars, 100 μm).

Inflammatory response and *in vivo* glyconanoparticles biodistribution in mice

The inflammatory response of the assembled glyco-nanoconjugates was evaluated by bronchoalveolar lavage (BAL) cell analysis. At steady state conditions, the most abundant cells retrieved in BAL fluid are the resident alveolar macrophages that line the alveolar space, (about 98% of BAL cells), and under inflammatory conditions infiltrating leukocytes such as lymphocytes and neutrophils. Consequently, evaluation of the number of BAL macrophages, lymphocytes and neutrophils was used to characterize the inflammatory response (**Figure 5**) upon treatment with PEGylated GlycoNPs and siRNA GlycoNPs in cancer mice during 1, 3 and 14 days. **Figure 5A** shows representative microscope images of BAL cells at day 1 and 14 for 200 μg/mL of PEGylated GlycoNPs and siRNA GlycoNPs. **Figure 5B** shows evaluation of the number of macrophages, lymphocytes and neutrophils in cancer mice during 1, 3 and 14 days after PEGylated GlycoNPs and siRNA GlycoNPs instillation. No multinucleated macrophages, indicators of a foreign body response are found at any condition. As expected[13], Sham treated group (healthy mice without lung cancer induction of luciferase-CMT/167 adenocarcinoma cells) reveals intact and normal alveolar macrophages (**Figure 5A**). Inflammatory cells infiltration is noted by increasing numbers of neutrophils in the siRNA GlycoNPs (200 μg/mL) treated groups on days 1 and 14 (**Figure 5A**). PEGylated and siRNA GlycoNPs show the same pattern and number of macrophages as well as neutrophils and lymphocytes (**Figure 5B**). The increased number of neutrophils with 200 μg/mL of PEGylated and siRNA GlycoNPs on day 1 indicates a moderate acute and over time rapidly declining inflammatory response, resulting in baseline levels (sham) and thus negligible neutrophil numbers at day 3 and 14 after treatment (**Figure 5B**). No significant changes have been observed for BAL lymphocyte numbers over the period of investigation, pointing to the generally described innate, acute inflammatory response to pulmonary deposited materials [32,33] No significant changes in the number of macrophages and neutrophils between PEGylated GlycoNPs and siRNA GlycoNPs are observed (**Figure 5B**).

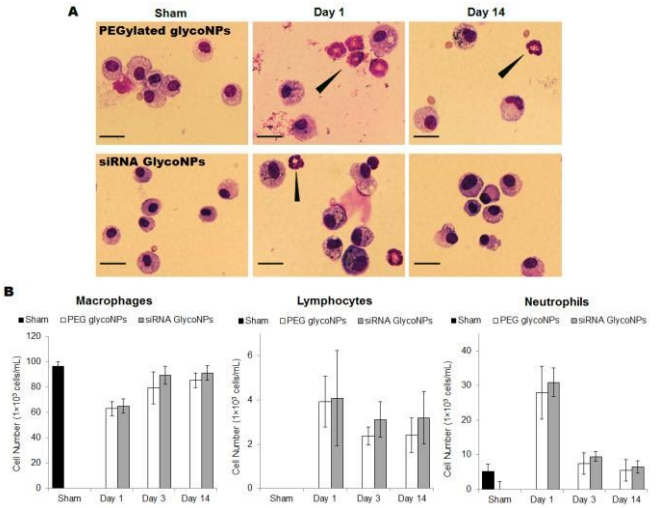

Figure 5. Inflammatory response in bronchoalveolar lavage (BAL) cells in mice during 1, 3 and 14 days of exposure to gold GlycoNPs. (**A**) Representative microscope images of BAL cells (scale bars, 20 μm) at days 1 and 14 for 200 μg/mL of PEGylated GlycoNPs and siRNA GlycoNPs. Black arrows indicate neutrophils. (**B**) Evaluation of the number of macrophages, lymphocytes and neutrophils was used to detect inflammatory response in the lungs during 1, 3 and 14 days after PEGylated GlycoNPs and siRNA GlycoNPs instillation. Sham groups correspond to healthy mice without lung cancer induction and any nanoparticle treatment. Error bars indicate ± s.d, of n=6 mice.

In order to analyse tumour size, nanoparticle uptake and biodistribution in the whole body mice but predominantly in lung tumour tissue, tomography bioluminescence imaging was carried out in the mouse cancer model (B6 albino female mice injected with luciferase-CMT/167 adenocarcinoma cells) treated with 200 μg/mL of PEGylated GlycoNPs and siRNA GlycoNPs (**Figure 6**). Representative whole body images of the individual mice from each treated group (n = 8 animals) shown at fixed photon flux scale illustrates the luciferase activity (**Figure 6A**). Detection of epi-fluorescence (**Figure 6B**) further allowed localization of nanoparticle conjugated to streptavidin with Cy7-Allophycocyanin (Cy7APC, BD Pharmingen™) with an excitation wavelength of at 642 nm. **Figures 6C** and **6D** shows excised organs to evaluate lung tumour size via the luminescence of luciferase and **Figures 6E** and **6F** shows nanoparticle distribution in mice organs via the measurement of epi-fluorescence of nanoparticles conjugated to streptavidin with Cy7-Allophycocyanin (Exc = 642 nm).

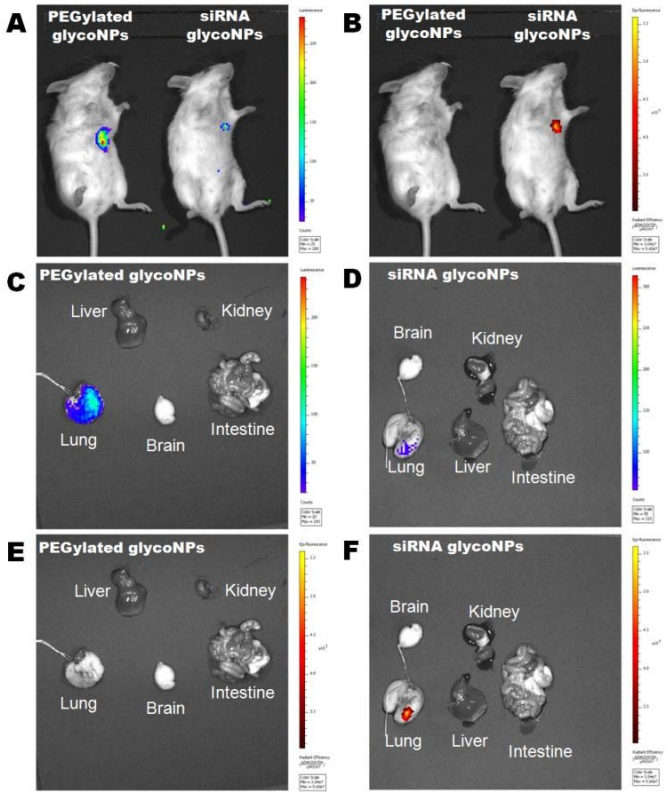

Figure 6. GlycoNPs uptake, whole body biodistribution and tumour size assessment in mice. Tomography imaging of B6 albino female mice injected with luciferase-CMT/167 adenocarcinoma cells (n = 8 animals per treated group) treated with 200 µg/mL of PEGylated GlycoNPs and siRNA GlycoNPs. Representative imaging of individual mice from each treatment group (n = 8 animals) is shown, with the same scale of photon flux indicating luciferase activity (**A**) and epi-fluorescence (**B**) indicating nanoparticles conjugated to streptavidin with Cy7-Allophycocyanin (Cy7APC, BD Pharmingen™) with an excitation wavelength of at 642 nm. (**A,B**) Luminescence and epi-fluorescence images of lung cancer mice treated with 200 µg/mL of PEGylated GlycoNPs and siRNA GlycoNPs. Excised organs to evaluate lung tumour size via the luminescence of luciferase in mice treated with PEGylated AuNPs (**C**) and gold GlycoNPs (**D**). Nanoparticle distribution indifferent organs treated with PEGylated GlycoNPs (**E**) and siRNA GlycoNPs (**F**), via the measurement of epi-fluorescence of nanoparticles conjugated to streptavidin with Cy7-Allophycocyanin.

The tomography images clearly depict that siRNA GlycoNPs archive an increased targeting toward lung cancer cells when compared to PEGylated GlycoNPs treatment, which shows no signal-accumulation in the respective lung tissue, for the same scale of epi-fluorescence. Once the lung is characterized by high expression of *c-Myc*, siRNA anti-*cMyc* targeting GlycoNPs seem to accumulate in the tissue more effectively and for a longer period of time than observed for PEGylated GlycoNPs only. Moreover, treatment of the murine lung cancer model with GlycoNPs leads to successful tumour size reduction (~80%) as depicted by the decrease in reporter luminescence signal (**Figure 6A,C**), when compared to the PEGylated GlycoNPs.

Experimental

Synthesis of PEGylated and siRNA GlycoNPs

Full description of synthesis and characterization methods of PEGylated GlycoNPs and siRNA GlycoNPs can be found in Supplementary Information.

Immunostaining of luciferase-CMT/167 adenocarcinoma cells

Cells were fixed with -20°C methanol for 10 min and with -20°C acetone for min on cover slips. The cover slips were washed twice in PBS, and then blocked with PBS containing 0.1% BSA for 10 min at room temperature followed by draining. The cell-side-up of glass slide was incubated with anti-rabbit Fas (Santa Cruz Biotechnology) in PBS containing 1% BSA for 60 min, and was washed three times in PBS. The samples were incubated with Alexa 546 anti-rabbit or FITC 488 anti-rabbit as the secondary antibody and phalloidin (Invitrogen), at the recommended dilution, in PBS containing 1% BSA, for 30 min, and then was washed for three times in PBS. After DAPI staining, one drop of aqueous mounting medium was added on the cover slip and inverted carefully on a glass slide. The images were acquired in a Zeiss confocal microscope and the fluorescent density per cell was analysed by ImageJ.

Western blot of Fas/CD95, caspase 3 and 9 expression

Protein extract was boiled in sample buffer for 3 min and loaded onto 12% SDS-polyacrylamide gels. Details of the Western immunoblotting procedure have been described elsewhere.[34] The antibodies used in this experiment were as follows: anti-rabbit Fas (Santa Cruz Biotechnology, 1:500 dilution), anti-rabbit Caspase3 (cleaved) (Invitrogen, 1:500 dilution), and anti-rabbit polyclonal Caspase9 (cleaved) (Abcam, 1:1000 dilution), anti-rabbit IgG horseradish peroxidase (Amersham-Pharmacia Biotech, 50000:1 dilution). The blot was visualized with an ECL kit (Amersham-Pharmacia Biotech).

In vivo targeting of PEGylated glycoNP and siRNA GlycoNPs

Prior to glycoNP instillation, B6 albino mice (B6N-Tyr^{c}/BrdCrCrl, Charles River, France, induced with luciferase-CMT/167 adenocarcinoma cells) were anesthetized by intraperitoneal injection of a mixture of Medetomidin (0.5 mg/kg body mass), Midazolam (5.0 mg/kg body mass) and Fentanyl (0.05 mg/kg body mass). The animals were then intubated by a nonsurgical technique. Using a cannula inserted 10 mm into the trachea, a suspension containing 1×10^{5} cancer cells or 200 µg/mL of PEGylated GlycoNPs and siRNA GlycoNPs, in 50 µl pyrogene-free distilled water was instilled, followed by 100 µl air. After instillation animals were antagonized by subcutaneous injection of a mixture of Atipamezol (2.5 mg/kg body mass), Flumazenil (0.5 mg/kg body mass) and Naloxon (1.2 mg/kg body mass) for antagonization and to control awakening of the mice. Animal experiments were carried out according to the German law of protection of animal life and were approved by an external review committee for laboratory animal care (animal approval number: 55.2-1-54-2532-20-11). After 72 hours mice lungs were dissected and prepared for Hematoxylin and Eosin staining (H&E) and for immunolocalisation by a standard immunohistochemical procedure, to verify *c-Myc* expression and the distribution of NPs by tissue sections.

Molecular analyses of MYC expression in mice

The lung cancer tissues (from B6 albino mice induced with luciferase-CMT/167 adenocarcinoma cells) were embedded and sliced into 3 µm section. A standard Hematoxylin and Eosin (H&E) staining was employed for cancer cells morphology observation. For immunolocalisation, standard immunohistochemical staining methods were employed: the tissue slide was incubated with anti-mouse *c-Myc* and anti-rabbit caspase-3, (1:1000) in PBS containing 1% BSA for 60 min, and was washed three times in Tris-buffered saline (TBS). The slide was incubated with 560 nm anti mouse and FITC anti-rabbit as the secondary antibody, at the recommended dilution, in TBS containing 1% BSA, for 30 min, and then was washed for three times in PBS. The slides were mounted with 50 µl of mounting medium. The images were acquired by a Zeiss confocal microscopy and the fluorescent density per cell analysed by ImageJ.

Preparation of BAL cells/fluid for evaluation of inflammatory response

BAL (bronchoalveolar lavage cells) fluid was obtained by injecting 4 times and recovering of two 0.5 mL aliquots of PBS via a tracheal cannula. Cells recovered with the lavage fluid (lymphocytes and neutrophils accompanying the predominant population of alveolar macrophages) were determined utilizing light microscopic cell differentiation, counting 200 cells per cytospin preparation. Details of the bronchoalveolar lavage procedure were described elsewhere.[35] Mice were exposed to 200 µg/mL of PEGylated GlycoNPs or siRNA GlycoNPs.

In vivo bioluminescence imaging

Stable clones of CMT64/61 cells, originally derived from a spontaneous lung adenocarcinoma of a C57Bl/ICRF mouse [32] were generated by transfection with pGL3-Control vector (Promega GmbH), and co-transfection for selection with a linear Hygromycin resistance marker (Clonetech). A stable clone (CMT/167-luc) expressing high levels of firefly luciferase, constitutively driven by the SV40 promoter and enhancer, was instilled into female C57BL/6 albino mice. Prior to instillation, mice were anesthetized by intraperitoneal injection of a mixture of Medetomidin (0.5 mg/kg body mass), Midazolam (5.0 mg/kg body mass) and Fentanyl (0.05 mg/kg body mass). The animals were then intubated by a nonsurgical technique. Using a cannula inserted 10 mm into the trachea, a suspension containing 1×10^5 CMT/167-luc cells in 50 µl pyrogene-free distilled water was instilled, followed by 100 µl of air, at week 8. Four weeks after orthotropic lung cancer induction mice were treated by instillation of 0.3 pmol AuNP (at weeks 12, 13, 14 and 15), respectively, in 50 µl pyrogene-free distilled water, followed by 100 µl of air. After instillation animals were antagonized by subcutaneous injection of a mixture of Atipamezol (2.5 mg/kg body mass), Flumazenil (0.5 mg/kg body mass) and Naloxon (1.2 mg/kg body mass). Luciferase expression was monitored applying the IVIS® imaging system (Lumina, PerkinElmer) from mice bearing tumours from luciferase-CMT/167 cells (n = 8 animals per treated group).

Conclusions

Several studies were published in the last years reporting that some engineered gold nanoparticles induce apoptosis in cells via caspase pathways. Herein, we present for the first time a new and smart RNAi-based gold glyconanoparticle system capable of inducing apoptosis via hyperactivation of cell death receptors and caspase pathways. In summary, we demonstrate that siRNA GlycoNPs have remarkable potential to trigger apoptosis via the enhancement of cell death receptors and activation of caspases. Moreover, our results confirm that sham, PEGylated GlycoNPs and siRNA GlycoNPs treated groups' causes the same inflammatory response, proving that siRNA GlycoNPs trigger apoptotic pathways via expression of cell death receptors and effective caspases in a specific way, independent from the inflammatory response. Consequently, the switch on of the apoptotic pathways is not caused by any toxic and/or adverse side effects of the exposure to the NPs in mice. Most importantly, pulmonary delivered of siRNA GlycoNPs leads to a ~80% reduction in tumour size via *in vivo* RNAi in tumour tissue by targeting *c-Myc* gene expression.

Acknowledgements

Authors thank ERANET-NANOSCIERA NANOTRUCK project for financial support. JMF thanks Fondo Social Europeo for financial support.

Notes and references

[a] Massachusetts Institute of Technology, Institute for Medical Engineering and Science, Harvard-MIT Division for Health Sciences and Technology, E25-449 Cambridge, Massachusetts, USA.

[b] Comprehensive Pneumology Centre, Institute of Lung Biology and Disease, Helmholtz Zentrum München, Neuherberg, Germany.

[c] Instituto de Nanociencia de Aragon (INA), Universidad de Zaragoza, Zaragoza, 50018, Spain

[d] Institute of Nano Biomedicine and Engineering, Key Laboratory for Thin Film and Microfabrication Technology of the Ministry of Education, Research Institute of Translation Medicine, Shanghai Jiao Tong University, Dongchuan Road 800, 200240 Shanghai, People's Republic of China.

[e] CIGMH, Departamento de Ciências da Vida, Faculdade de Ciências e Tecnologia, Universidade Nova de Lisboa, Campus de Caparica, 2829-516 Caparica, Portugal.

[f] Instituto de Ciencia de Materiales de Aragón-CSIC/Universidad de Zaragoza, Spain

† Both authors have contributed equally to this manuscript

* Corresponding authors: tobias.stoeger@helmholtz-muenchen.de & jmfuente@unizar.es

Electronic Supplementary Information (ESI) available: Synthesis, functionalization and quantification methods for siRNA-gold glyconanoparticles. See DOI: 10.1039/b000000x/

1 C. M. Dong, Glyconanoparticles for biomedical applications, *Comb Chem High Throughput Screen*. 2011, **14**, 173-181.

2 J. M. de la Fuente, S. Penades, Understanding carbohydrate-carbohydrate interactions by means of glyconanotechnology, *Glycoconjugate Journal*. 2004, **21**, 149-163.

3 J. M. de la Fuente, A. G. Barrientos, T. C. Rojas, J. Rojo, J. Canada, A. Fernandez, S. Penades, Gold glyconanoparticles as water-soluble polyvalent models to study carbohydrate interactions, *Angewandte Chemie-International Edition*. 2001, **40**, 2258-2261.

4 A. G. Barrientos, J. M. de la Fuente, T. C. Rojas, A. Fernandez, S. Penades, Gold glyconanoparticles: Synthetic polyvalent ligands mimicking glycocalyx-like surfaces as tools for glycobiological studies, *Chemistry-A European Journal*. 2003, **9**, 1909-1921.

5 J. M. de la Fuente, S. Penades, Glyconanoparticles: types, synthesis and applications in glycoscience, biomedicine and material science, *Biochim Biophys Acta*. 2006, **1760**, 636-651.

6 J. M. de la Fuente, D. Alcantara, P. Eaton, P. Crespo, T. C. Rojas, A. Fernandez, A. Hernando, S. Penades, Gold and gold-iron oxide magnetic glyconanoparticles: synthesis, characterization and magnetic properties, *J Phys Chem B*. 2006, **110**, 13021-13028.

7 J. Rojo, V. Diaz, J. M. de la Fuente, I. Segura, A. G. Barrientos, H. H. Riese, A. Bernade, S. Penades, Gold glyconanoparticles as new tools in antiadhesive therapy, *Chembiochem*. 2004, **5**, 291-297.

8 J. M. de la Fuente, P. Eaton, A. G. Barrientos, M. Menendez, S. Penades, Thermodynamic evidence for Ca2+-mediated self-aggregation of Lewis X gold glyconanoparticles. A model for cell adhesion via carbohydrate-carbohydrate interaction, *Journal of the American Chemical Society*. 2005, **127**, 6192-6197.

9 M. Reynolds, M. Marradi, A. Imberty, S. Penades, S. Perez, Multivalent Gold Glycoclusters: High Affinity Molecular Recognition by Bacterial Lectin PA-IL, *Chemistry-A European Journal*. 2012, **18**, 4264-4273.

10 C. L. Schofield, A. H. Haines, R. A. Field, D. A. Russell, Silver and gold glyconanoparticles for colorimetric bioassays, *Langmuir*. 2006, **22**, 6707-6711.

11 J. Conde, A. Ambrosone, V. Sanz, Y. Hernandez, V. Marchesano, F. Tian, H. Child, C. C. Berry, M. R. Ibarra, P. V. Baptista, C. Tortiglione, J. M. de la Fuente, Design of Multifunctional Gold Nanoparticles for In Vitro and In Vivo Gene Silencing, *ACS Nano*. 2012, **6**, 8316–8324.

12 V. Sanz, J. Conde, Y. Hernandez, P. V. Baptista, M. R. Ibarra, J. M. de la Fuente, Effect of PEG biofunctional spacers and TAT peptide on dsRNA loading on gold nanoparticles, *Journal of Nanoparticle Research*. 2012, **14**.

13 J. Conde, F. Tian, Y. Hernandez, C. Bao, D. Cui, K. P. Janssen, M. R. Ibarra, P. V. Baptista, T. Stoeger, J. M. de la Fuente, In vivo tumor targeting via nanoparticle-mediated therapeutic siRNA coupled to inflammatory response in lung cancer mouse models, *Biomaterials*. 2013, **34**, 7744-7753.

14 K. Maedler, G. A. Spinas, R. Lehmann, P. Sergeev, M. Weber, A. Fontana, N. Kaiser, M. Y. Donath, Glucose induces beta-cell apoptosis via upregulation of the Fas receptor in human islets, *Diabetes*. 2001, **50**, 1683-1690.

15 R. W. Y. Yeo, K. Y. Yang, G. D. Li, S. K. Lim, High Glucose Predisposes Gene Expression and ERK Phosphorylation to Apoptosis and Impaired Glucose-Stimulated Insulin Secretion via the Cytoskeleton, *Plos One*. 2012, **7**.

16 M. Lorenzi, D. F. Montisano, S. Toledo, A. Barrieux, High Glucose Induces DNA Damage in Cultured Human-Endothelial Cells, *Journal of Clinical Investigation*. 1986, **77**, 322-325.

17 M. Lorenzi, E. Cagliero, S. Toledo, Glucose Toxicity for Human-Endothelial Cells in Culture - Delayed Replication, Disturbed Cell-Cycle, and Accelerated Death, *Diabetes*. 1985, **34**, 621-627.

18 M. Lopez-Lazaro, The warburg effect: why and how do cancer cells activate glycolysis in the presence of oxygen? *Anticancer Agents Med Chem*. 2008, **8**, 305-312.

19 J. Turkevich, P. C. Stevenson, J. Hillier, A study of the nucleation and growth processes in the synthesis of colloidal gold. *Discussions of the Faraday Society*. 1951, **11**, 55-75

20 G. Frens, Controlled Nucleation for the Regulation of the Particle Size in Monodisperse Gold Suspensions. *Nature physical science*. 1973, **241**, 20-22.

21 X. Zhang, V. K. Yadavalli, Functionalized self-assembled monolayers for measuring single molecule lectin carbohydrate interactions. *Analytica Chimica Acta*. **649**, 1-7.

22 D. N. Boone, Y. Qi, Z. L. Li, S. R. Hann, Egr1 mediates p53-independent c-Myc-induced apoptosis via a noncanonical ARF-dependent transcriptional mechanism, *Proceedings of the National Academy of Sciences of the United States of America*. 2011, **108**, 632-637.

23 S. Y. Lunt, M. G. Vander Heiden, Aerobic Glycolysis: Meeting the Metabolic Requirements of Cell Proliferation, *Annual Review of Cell and Developmental Biology*, 2011, **27**, 441-464.

24 S. Elmore, Apoptosis: A review of programmed cell death, *Toxicologic Pathology*. 2007, **35**, 495-516.

25 J. C. Mohan, G. Praveen, K. P. Chennazhi, R. Jayakumar, S. V. Nair, Functionalised gold nanoparticles for selective induction of in vitro apoptosis among human cancer cell lines, *Journal of Experimental Nanoscience*. 2013, **8**, 32-45.

26 H. K. Patra, S. Banerjee, U. Chaudhuri, P. Lahiri, A. K. Dasgupta, Cell selective response to gold nanoparticles, *Nanomedicine-Nanotechnology Biology and Medicine*. 2007, **3**, 111-119.

27 W. Gao, K. H. Xu, L. F. Ji, B. Tang, Effect of gold nanoparticles on glutathione depletion-induced hydrogen peroxide generation and apoptosis in HL7702 cells, *Toxicology Letters*. 2011, **205**, 86-95.

28 P. Mukherjee, R. Bhattacharya, N. Bone, Y. K. Lee, C. R. Patra, S. Wang, L. Lu, C. Secreto, P. C. Banerjee, M. J. Yaszemski, N. E. Kay, D. Mukhopadhyay, Potential therapeutic application of gold nanoparticles in B-chronic lymphocytic leukemia (BCLL): enhancing apoptosis, *J Nanobiotechnology*. 2007, **5**, 4.

29 B. Kang, M. A. Mackey, M. A. El-Sayed, Nuclear Targeting of Gold Nanoparticles in Cancer Cells Induces DNA Damage, Causing Cytokinesis Arrest and Apoptosis, *Journal of the American Chemical Society*. 2010, **132**, 1517-1519.

30 I. C. Sun, S. Lee, H. Koo, I. C. Kwon, K. Choi, C. H. Ahn, K. Kim, Caspase Sensitive Gold Nanoparticle for Apoptosis Imaging in Live Cells, *Bioconjugate Chemistry*. 2010, **21**, 1939-1942.

31 G. C. Prendergast, Mechanisms of apoptosis by c-Myc, *Oncogene*. 1999, **18**, 2967-2987.

32 A. Beyerle, A. Braun, A. Banerjee, N. Ercal, O. Eickelberg, T. H. Kissel, T. Stoeger, Inflammatory responses to pulmonary application of PEI-based siRNA nanocarriers in mice, *Biomaterials*. **2011**, 32, 8694-701.

33 K. Ganguly, S. Upadhyay, M. Irmler, S. Takenaka, K. Pukelsheim, J. Beckers, E. Hamelmann, H. Schulz, T. Stoeger, Pathway focused protein profiling indicates differential function for IL-1B, -18 and VEGF during initiation and resolution of lung inflammation evoked by carbon nanoparticle exposure in mice, *Part Fibre Toxicol.* **2009**, 6.

34 J. G. Steele, C. Rowlatt, J. K. Sandall, L. M. Franks, Cell-Surface Properties of High-Metastatic and Low-Metastatic Cell-Lines Selected from A Spontaneous Mouse Lung-Carcinoma, *International Journal of Cancer*. **1983**, 32, 769-779.

35 F. R. Tian, T. Nakahara, M. Yoshida, N. Honda, H. Hirose, J. Miyakoshi, Exposure to power frequency magnetic fields suppresses X-ray-induced apoptosis transiently in Ku80-deficient xrs5 cells, *Biochemical and Biophysical Research Communications*. 2002, **292**, 355-361.